

---

# Navigating the Latent Space Dynamics of Neural Models

---

Marco Fumero\*  
IST Austria

Luca Moschella†  
Sapienza

Emanuele Rodolà‡  
Sapienza

Francesco Locatello‡  
IST Austria

## Abstract

Neural Network (NN) transform high-dimensional data into compact, structured representations, often modeled as elements of a lower dimensional latent space. In this paper, we present an alternative interpretation of neural models as dynamical systems acting on the latent manifold. Specifically, we show that AutoEncoder (AE) models implicitly define a *latent vector field* on the manifold, derived by iteratively applying the encoding-decoding map, without any additional training. We observe that standard training procedures introduce inductive biases that lead to the emergence of attractor points within this vector field. Drawing on this insight, we propose to leverage the vector field as a *representation* for the network, providing a novel tool to analyze the properties of the model and the data. This representation enables to: (i) analyze the generalization and memorization regimes of neural models, even throughout training; (ii) extract prior knowledge encoded in the network’s parameters from the attractors, without requiring any input data; (iii) identify out-of-distribution samples from their trajectories in the vector field. We further validate our approach on vision foundation models, showcasing the applicability and effectiveness of our method in real-world scenarios.

## 1 Introduction

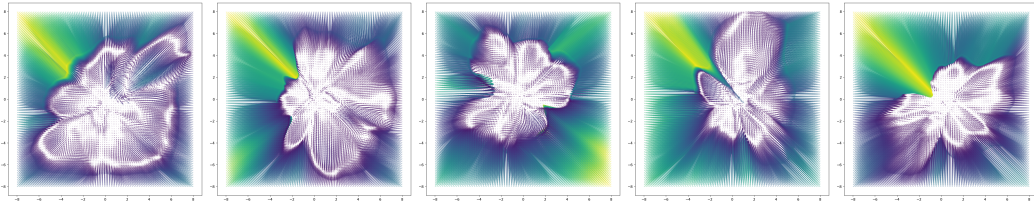


Figure 1: *The latent dynamics of AEs* Latent vector fields with  $\mathbf{z}_0 \sim \mathcal{U}[-8, 8]$  of 2D AEs trained on the MNIST dataset with different initializations. Colors denote the norm of the vectors: the boundary denotes the shape of the latent manifold identified with the support of the encoder, in white we observe regions of the latent space where the vector field vanishes, flowing toward attractors, which correspond to regions of high probability density of the data.

Neural models are effective function approximators that have been demonstrated to be able to solve complex tasks in countless domains [23, 41]. These models typically learn to transform high-dimensional data into compact, structured representations [4], often modeled as elements of a lower

---

\*Corresponding email: marco.fumero@ist.ac.at

†Currently at Apple.

‡Equally advising

dimensional latent space. In this work, we propose a novel alternative representation for neural models by showing that, for a given AE architecture, there exists an associated *latent vector field* (see Figure 1), which characterizes the behavior of the network at the representation level. The vector field is obtained by simply iterating the encoding decoding map in the latent space, without any additional training procedures. Previous work [42, 22] has demonstrated that in the extreme overparametrized regime and under strong assumptions, AEs can effectively memorize training data. In this work, we propose to consider the more general case in which memorization corresponds to one extremum, showing evidence that the latent vector field induced by general AEs can be reconnected to properties of the network, such as generalization, memorization, and out-of-distribution detection. Our contributions can be summarized as follows:

- We show that every AE architecture induces a latent vector field, implicitly. We demonstrate that this representation retains properties of the networks and the data, throughout its trajectories and its fixed points.
- We show that most mappings learned by NNs are contractive: this enforces the presence of fixed points and attractors points in the latent vector field.
- We empirically show how attractors characterize the memorization and generalization regime in NNs and their interplay in the training process.
- We experimentally demonstrate the information stored in vision foundation models weights can be retrieved in a data-free way, by probing models with noise and retrieve attractors.
- Finally, we show that paths in the latent vector fields are informative to characterize the learned distribution and to detect distribution shifts.

## 2 Method

**Notation and background** In the following sections we will consider neural models  $F$  as a composition of encoder decoder modules  $F_\Theta = D_{\theta_2} \circ E_{\theta_1}$  parametrized by  $\Theta = [\theta_1, \theta_2]$ . The encoder maps samples  $\mathbf{x} \sim p(\mathbf{x})$  supported on  $\mathcal{X} \subset \mathbb{R}^m$  to a typically lower dimensional space  $\mathcal{Z} \subset \mathbb{R}^k$  and the network  $F$  is trained for reconstruction to minimize the mean squared error  $\mathcal{L}_{MSE}$ :

$$\mathcal{L}_{MSE}(\mathbf{x}) = \sum_{\mathbf{x} \in \mathcal{X}} \|\mathbf{x} - F_\Theta(\mathbf{x})\|_2^2 + \lambda \mathcal{R}(\Theta) \quad (1)$$

where  $\mathcal{R}$  is either an explicit (e.g., weight decay) or implicit regularization constraint on the parameters  $\Theta$  to favor contractive solutions of  $F$ . We posit that minimizers of the above objective act as minimizers of the spectral norm of the Jacobian  $\rho(J_F(x))$  for  $x \sim p(x)$ . Some examples of regularizer include weight decay, where  $\mathcal{R} = \|\Theta\|_2^F$  or the use of some augmentations distribution  $p(T)$ , for which the objectives becomes:

$$\mathcal{L}_{MSE}(\mathbf{x}) = \sum_{\mathbf{x} \in \mathcal{X}} \|\mathbf{x} - F(\mathbf{x})\|_2^2 + \sum_{T \in p(T)} \|\mathbf{x} - F(T\mathbf{x})\|_2^2 \quad (2)$$

examples of  $p(T)$  include additive gaussian noise in denoising AEs [52] or masking, in masked AEs [15]. The bottleneck dimension  $k = \dim(\mathcal{Z})$  is another example of how to enforce a contractive behavior in the network. More precisely, the bottleneck dimension acts as a hard constraint on the rank of the Jacobian of the encoder  $\text{rank}(J_E) \leq k$  and therefore of the entire map  $F$ , since  $J_F(\cdot) = J_E(\cdot) \odot J_D(\cdot)$ . In Table 2 in the Appendix, we list many AE variants including denoising AEs (DAEs) [52], sparse AEs (SAEs) [37], variational AEs (VAEs) [26] and other variants [44, 2, 12] and show how their objectives enforce local contractive solutions around training points.

Given an AE model  $F$  possibly pretrained, denoting with  $f(\mathbf{z}) = E \circ D(\mathbf{z})$ , we are interested in analyzing the iterations of the map  $f(\dots f(f(\mathbf{z})))$ , which can be modeled as a differential equation.

### 2.1 The Latent Dynamics of Neural Models

For a sample  $\mathbf{z} \in \mathcal{Z} \subseteq \mathbb{R}^k$  we analyze the effect of applying iteratively  $f$  on  $\mathbf{z}$ , i.e.  $f \circ f \circ \dots f(\mathbf{z})$ . Parametrizing the number of iteration by  $t$ , this lead to the following discrete ordinary differential equation (ODE):

$$\begin{cases} \mathbf{z}_{t+1} = f(\mathbf{z}) \\ \mathbf{z}_0 = \mathbf{z} \end{cases} \quad (3)$$

which discretizes the following continuous differential equation:

$$\frac{\partial \mathbf{z}}{\partial t} = f(\mathbf{z}) - \mathbf{z} \quad (4)$$

In Eq 3, one can associate the map  $f$  as the pushforward of a *latent vector field*  $V : \mathbb{R}^k \mapsto \mathbb{R}^k$  tracing non linear trajectories in the latent space (see Fig 1). A first interesting question is whether this ODE has solutions and if they are unique. Through the Banach fixed point theorem, it can be shown that the ODE has a unique solution iff the map  $f$  is Lipschitz continuous.

**Definition 1.** A function  $f : \mathcal{Z} \mapsto \mathcal{Z}$  is denoted *Lipschitz continuous* if there exist a constant  $C$  s.t. for every pair of points  $\mathbf{z}_1, \mathbf{z}_2$ :

$$d(\mathbf{z}_1, \mathbf{z}_2)_{\mathcal{X}} \leq C d(f(\mathbf{z}_1), f(\mathbf{z}_2))_{\mathcal{X}} \quad (5)$$

when  $C < 1$   $f$  is called *contractive*.

For any contractive map, there will exist fixed point solutions of Eq 3, i.e., iteratively applying the map  $f$  will converge to a unique constant solution via solving  $\mathbf{z}^* = f(\mathbf{z}^*)$ . The fixed point  $\mathbf{x}$  solutions correspond to singular points that attract and summarize the dynamics of the system.

**Definition 2.** A fixed point  $\mathbf{x} = f(\mathbf{x})$  is an *attractor* of a differentiable map  $f$  if all eigenvalues of the Jacobian  $J$  of  $f$  at  $\mathbf{x}$  are strictly less than one in absolute value.

When  $f$  is nonlinear, the ODE in Eq. 3 can have multiple solutions depending on the initial conditions  $\mathbf{z}_0$ . The previous definition allows for a definition of Lipschitz continuity which is inherently local:

**Definition 3.** Let function  $f : \mathcal{Z} \mapsto \mathcal{Z}$ . Let  $f$  also be differentiable and  $C$ -Lipschitz continuous. Then the Lipschitz constant  $C$  is given by:  $C = \sup_{\mathbf{z} \in \mathcal{Z}} \|J_{\mathbf{z}} f\|$ , where  $J_{\mathbf{z}} f$  is the Jacobian of  $f$  w.r.t. to input  $\mathbf{z}$  and  $\|\cdot\|$  is the spectral norm.

The set of initial conditions  $\mathcal{Z}_0$  leading to the same attractor  $\mathbf{z}^*$ , is denoted as *basin of attraction*.

**Why maps learned by NNs are contractive in practice?** We argue that most maps learned by neural AEs or variants thereof, promote (locally) contractive autoencoding mappings. In other words, many explicit or implicit regularization strategies and training design choices constrain the Jacobian of the autoencoding map to have small eigenvalues near training examples. We provide below what are the inductive biases that promote locally contractive mappings:

- **Initialization** Standard initialization schemes [29, 14, 16] aim at preserving the variance of the activations at initialization to avoid gradient vanishing and exploding problems during training. Theoretical arguments in support assume i.i.d. input samples and weights, and are generally tied to specific activation functions (e.g., ReLU in [16]). We note that in practice, this condition is not likely to hold, as training data samples are often correlated and many employed architectural elements (for example, residual connections [17]) break the independence assumptions of the layer weights. Networks result in a bias to be either expansive or contractive towards a single point, with a preference for the latter case [39]. We show empirically that this is indeed the case in Figure 6 in the Appendix, across several vision backbone models. In Figure 3, we show an example of a 2D latent vector field which is globally contractive at initialization (Figure 3a, left plot) towards a single attractor at the origin. This is the case even in higher dimensions (see the number of attractors at the first epoch in Figure 3c).
- **Explicit regularization** Widely employed regularization techniques such as weight decay [7], implicitly constraints the learned map to be (locally) contractive. This can be seen easily in the case of linear mappings, where penalizing the norm of the matrix corresponds to penalizing the first-order derivatives of the map, resulting in the optimal way to make the map contractive. Although this is not guaranteed to be optimal for nonlinear networks, weight decay still enforces a contraction mapping. The regularizer is incorporated in state-of-the-art optimizers [32], ubiquitous in state-of-the-art foundation models. Other forms of parametric constraints include the choice of bottleneck dimension, which acts as a hard constraint on the rank of  $J_F(\mathbf{z})$ , and soft variants thereof, such as the Kullback-Leibler divergence term in VAEs, or sparsity regularization in SAEs.
- **Implicit regularization** As previously discussed, the choice of augmentation distribution implicitly selects the notion of neighborhood of the training samples (for example, Gaussian radius in DAEs), and the perturbation direction that will be penalized in  $J_f(\mathbf{x})$ . This form of regularization is nonparametric and inherently local as opposed to the explicit regularization techniques explained in the above paragraph.

### 3 Theoretical remarks

In this section, we are interested in analyzing properties of trajectories within the latent vector field, as well as its fixed points and attractors, when they exist.

#### 3.1 Trajectories of the latent vector field

In [2, 34, 45], it was shown that, under optimal conditions, the residual in denoising AEs trained with noise variance  $\sigma^2$  approximates the score function, i.e., the gradient of the log empirical density of the data, as  $\sigma \rightarrow 0$ . Interestingly, [2] shows a connection between denoising and contractive AEs, where the norm of the Jacobian of the input-output mapping is penalized. The more general result we want to stress here is that whenever the auto-encoding map is locally contractive w.r.t. a given notion of neighborhood (e.g. gaussian radius, masking augmentations) and approximates well enough the input distribution  $p(\mathbf{x})$ , then the associated latent vector field pushes samples in the direction of the derivative of the score of the approximated prior in the latent space. Informally, this means that the vector field will non-linearly project samples on the data manifold onto regions of high probability density.

**Theorem 1.** (informal) *Let  $F$  be a trained AEs and let  $q(\mathbf{z}) = \int p(\mathbf{x})q(\mathbf{z}|\mathbf{x})d\mathbf{x}$  be the marginal distribution in the latent space induced by the AEs. Under assumptions on  $q(\mathbf{z})$  and if there exists an open neighborhood  $\Omega \supseteq \text{supp } q$  and a constant  $L < 1$  such that  $\sup_{z \in \Omega} \|J_f(z)\|_{\text{op}} \leq L$ , the latent dynamics  $f(\mathbf{z}) - \mathbf{z}$  around  $\Omega$  is proportional to the score function  $\nabla_{\mathbf{z}} \log q_{\Theta_1}(\mathbf{z})$ .*

This result is a general statement that connects paths in the vector field with the score, by assuming that the map is locally contractive. In practice, we argue that NNs achieve a trade-off between the reconstruction term of the loss in Eq 1 and the regularization term on the Jacobian, which contributes to the formation of attractors. An important consequence of Theorem 1 is that, when it holds, integrating the vector field  $f(\mathbf{z}) - \mathbf{z}$  corresponds to estimating the log density  $\log q(\mathbf{z})$ , i.e.  $\int_{\mathbf{z}} \nabla \log q(\mathbf{z}) d\mathbf{z} = \log q(\mathbf{z}) + C$  for unbounded domains. In the case  $J_f$  is symmetric (a practical example is the case of an AEs with tied weights [1]), then the latent vector field is *conservative* and corresponds to the gradient of a potential  $V_f = \nabla E$ . In this specific case, the resulting AEs defines an energy-based model  $q(\mathbf{z}) = e^{-E(\mathbf{z})}$  [55, 49]. In the general case, we show how the trajectories in the vector field are informative in capturing the learned prior distribution in our experiments in section 4.2.

In general, attractors cannot be computed via solving the fixed point equation with first-order methods, unless the initial condition is arbitrary close to the attractors, as the following result shows:

**Proposition 3.1.** *Iterations of the map  $f$  in Equation 3 correspond to performing gradient descent in the  $\frac{\partial L(\mathbf{z})}{\partial \mathbf{z}}$  iff  $f$  is an isometry (i.e. its eigenvalues are concentrated near 1) or in the proximity of attractor points, when the Jacobian of  $f$  vanishes.*

This result highlights the importance of the higher order terms involved in iterating  $f$ , which trace a highly nonlinear trajectory in latent space, escaping local minima solutions given by unstable and spurious fixed points.

#### 3.2 Characterizing the attractors of the latent vector field

In this section we aim to characterize what the fixed point solution of Eq 3 represents. We start by considering two base cases:

**Linear maps** In the linear case, the encoding map  $E$  and decoding  $D$  are parametrized by matrices  $\mathbf{W}_1 \in \mathbb{R}^{N \times k}$  and  $\mathbf{W}_2 \in \mathbb{R}^{k \times N}$  and the only fixed point of the map corresponds to the *origin* if the network is bias free or to a shift of it. The rate of convergence of the iteration in Eq 3 is established by the spectrum of  $\mathbf{W}_2^T \mathbf{W}_1$ , and the iteration is equivalent to shrinking the input in the direction of the eigenvectors with associated eigenvalue  $\lambda < 1$ . In case the eigenvectors of the trained AEs are aligned with the optimal solution given by the Principal Component Analysis (PCA) decomposition of the data  $\mathbf{X} = \Phi \Lambda \Phi^*$ , then the latent vector field vanished as the mapping is isometric and no contraction occurs.

**Homogeneous maps** In the case of homogeneous NNs, the network satisfies  $F(c\mathbf{x}) = c^\alpha F(\mathbf{x})$  with  $c \in \mathbb{R}$  for some  $\alpha$ . For example, this holds for ReLU networks without biases with  $\alpha = 1$ , which

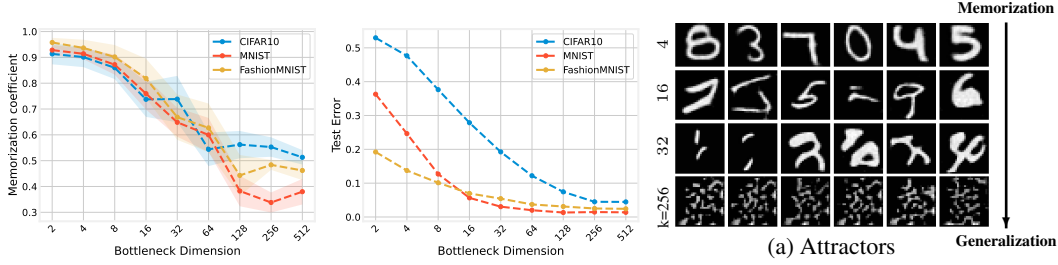


Figure 2: *Memorization vs Generalization*: Attractors memorize the training data as a function of the rank of  $J_f(\mathbf{z})$  by adjusting the bottleneck dimension  $k$  (Left); which is inversely proportional to the amount of generalization attained by the model (center); On the right we show example of attractors transition from a strong memorization model (First row), to good generalization (Last row).

learn a piecewise linear mapping. The input-output mapping can be rewritten as:

$$F(\mathbf{x}) = J_F(\mathbf{x})\mathbf{x} \quad (6)$$

A similar observation was made in for denoising networks in [24], we remark here its generality.

This equality implies that we can rewrite Equation 3 as :

$$\mathbf{z}_{t+1} = J_f(\mathbf{z}_t)\mathbf{z}_t = \sum_i \lambda_i \phi_i \mathbf{z}_t \quad (7)$$

Where  $\sum_i \lambda_i \phi_i$  is the eigendecomposition of  $J_f(\mathbf{z})$ . Since in the proximity of an attractor  $\max \lambda(J_F(\mathbf{z}^*)) \leq 1$ , the iterations shrink directions corresponding to the eigenvectors of the Jacobian by the corresponding eigenvalue. This allows us to derive the following result on the speed of convergence.

**Proposition 3.2.** *The error  $e_t = \|\mathbf{z}_t - \mathbf{z}^*\|$  converge exponentially to an  $\epsilon$  depending on the spectral norm  $\rho(J_f(\mathbf{z}^*))$ , according to the formula  $\frac{\log(\frac{\epsilon}{\|\mathbf{e}_0\|})}{\log(\|\rho(J_f(\mathbf{z}^*))\|)}$  that provides an estimate for the number of iterations  $T$  to converge to the attractor.*

In Figure 11 in the Appendix, we measure how well the convergence formula predicts the measured number of iterations to converge to an attractor, on a fully non linear AEs with biases, where the assumptions of the current section are less likely to hold. The error in the estimate will be higher, when the initial condition  $\mathbf{z}_0$  is far from the attractor, as higher order terms dominate the dynamics, and the first order Taylor approximation accumulates more error.

**Extreme overparametrization case** When the capacity of a network exceeds the number of training examples by far, AEs enter in a overfitting regime which leads to data memorization [56, 42, 22, 24]. The network in this case learns a constant function or an approximation thereof, which can be retrieved through the iterations in Eq:3.

**Between memorization and generalization** Our goal is to characterize the properties of the latent vector field and the learned attractors in the general setting. We argue that different models can perfectly fit training points reaching similar low loss, but interpolate *differently* outside the training support, depending on the regularization strength and the amount of overparametrization. In this context, which information do  $\mathbf{z}^*$  store in general? We argue that neural models fall in a spectrum between memorization and generalization, depending on the strength of the regularization term in 1, and we hypothesize that attractors fully characterize where in the spectrum a model is. We consider attractors as *representations summarizing the information stored in the weights of the network*. This interpretation is in line with the convergences to modes of Theorem 3.1 and can be easily seen in the case of memorization. Specifically, we assume that attractors form a dictionary of  $N$  signals  $\mathcal{D}^* = \{\mathbf{z}_1^*, \dots, \mathbf{z}_P^*\}$  from a set of initial conditions sampled from an input distribution  $P_0$ . The dictionary corresponds to, possibly nonlinear, interpolations of the training data  $X$ , therefore  $\mathcal{D}^* = \Phi(X)$ . In the memorization regime,  $\Phi$  corresponds to the standard basis up to permutations, and the network approximates a constant function which can be retrieved through the iterations of Equation 3. Transitioning to a generalization regime  $\Phi$  can become arbitrarily complex. We demonstrate the interplay between memorization and generalization empirically in the experimental sections below. In Figure 2, we show how a model transitions from memorization to generalization

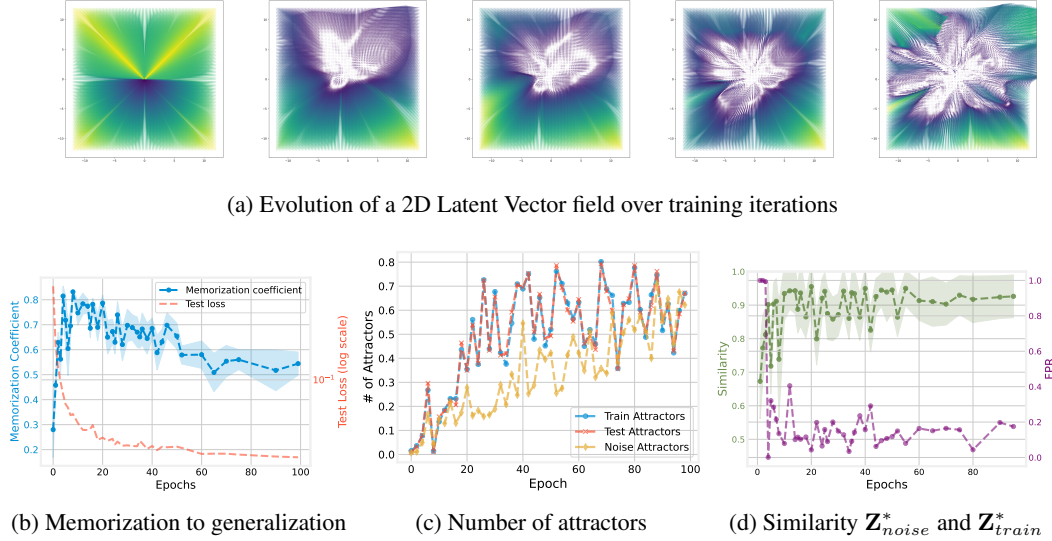


Figure 3: *The dynamics of the latent vector field* (a) The 2D vector field expands from a single attractor, eventually stabilizing and over-fitting because of capacity limits. *Bottom:* Evolution of larger capacity AEs ( $k = 128$ ) across training. (b) Throughout training, the network first memorizes the data with a high memorization coefficient (in blue) and then generalizes, achieving a low test error (red). (c): Evolution of attractor count for training (blue), test (red), and noise (yellow) samples; (d) Attractors computed from training and from gaussian noise converge during training (green), while the separability of the trajectories (measured as FPR95, the lower the better) increase (purple).

according to the strength of the regularization on  $J_f(\mathbf{z}^*)$ , by measuring how many training examples are stored as attractors. We remark that this memorization corresponds to an *over regularized* regime, as opposed to the *overfitting* regime of extremely overparametrized networks.

**Setting** We trained 30 convolutional AEs models on the CIFAR, MNIST, and FashionMNIST datasets, varying the bottleneck dimension  $k$  from 2 to 512. This acts as a hard regularizer on  $J_f(\mathbf{x}^*)$ , by constraining its rank to be  $\leq k$ . We compute attractors  $\mathbf{Z}^*$  from elements of the training set  $\mathcal{X}_{train}$  by iterating  $\mathbf{z}$  till convergence. We measure the degree of memorization by defining a *memorization coefficient*, which is given by the cosine similarity of each decoded attractor  $\mathbf{x}^* = D(\mathbf{z}^*)$  to its closest point in the training set,  $mem(\mathbf{z}^*) = \min_{\mathbf{x} \in \mathcal{X}_{train}} \cos(D(\mathbf{z}^*), \mathbf{x})$  and we report the mean and standard deviation over attractors. We measure generalization by simply reporting the error on the test set. In Figure 12 in the Appendix, we also report the rank explaining 90% of the variance of the matrix of decoded attractors  $\mathbf{X}^*$ , showing that attractors corresponding to good generalization models span more directions in the input space. For additional information on the model, hyperparameters, and settings, we refer to the Appendix.

**Analysis of results** In Figure 2 on the left, we observe that the more regularized networks ( $k$  from 2 to 16) tend to memorize data, trading off generalization performance (middle plot). We remark that this kind of memorization is not due to overfitting, as was shown in [24] for diffusion models, but it happens in the underfit regime, due to the strong regularization constraint on  $J_f(\mathbf{x})$ . We show in the Appendix results in the overfitting regime, by training the models with different sample sizes and observing a similar pattern.

**Takeaway:** Attractors capture the interplay between generalization and memorization of neural models, which corresponds to the trade-off between the reconstruction performance and regularization term of the AEs model.

In Figure 3 we show a similar transition from a memorization regime to generalization across training. **Setting** We monitor the latent vector field and attractors statistics across the training dynamics of a convolutional AEs trained on the MNIST with bottleneck dimension  $k = 128$ .

**Analysis of results** In Figure 3b we show the transition from memorization, occurring at the first epochs of training, to generalization, by plotting the memorization coefficient and the test error across training, observing a trade off between the two. In the central plot, we plot the fraction of distinct

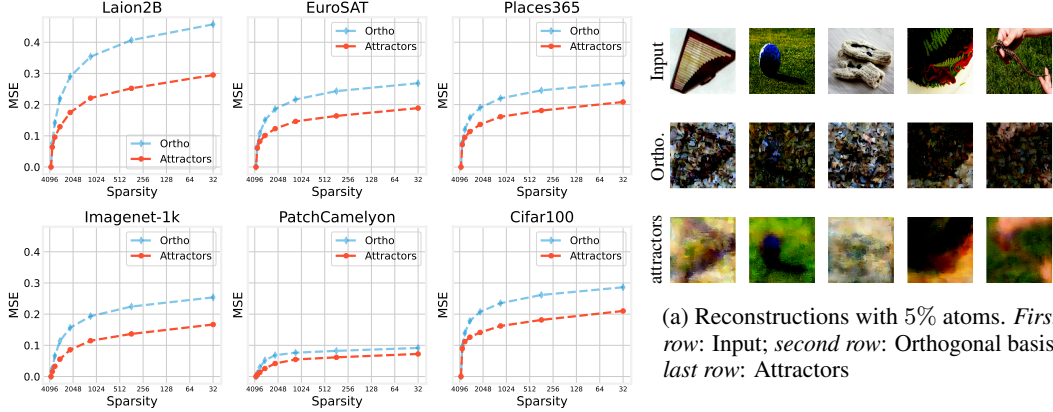


Figure 4: *Data-free weight information probing of Stable Diffusion model*: We plot the error (MSE) vs sparsity (number of atoms) used to reconstruct samples from diverse dataset respectively from (i) an orthonormal random basis of the latent space (*blue*); (ii) attractors computed from gaussian noise (*red*), showing that attractors consistently reconstructs samples better on all datasets. (*Right*) Reconstructions using 5% of the atoms on ImageNet

attractors, computed from 5000 random elements respectively from the  $P_{train}, P_{test}$  and  $\mathcal{N}(0, I)$ , where we consider two attractors equal if  $\cos(\mathbf{z}_1^*, \mathbf{z}_2^*) > 0.99$ . We observe that the number of attractors grows across epochs starting from a single attractor at initialization, as we can also observe in the 2d case in Figure 3a, with the training and test number of attractors stabilizing according to the test loss and the noise ones converging later. On the right, we plot the similarity of attractors computed from the training and the noise distributions, measured by Chamfer symmetric similarity, observing that it increases across training, as the two distributions of attractors match. Despite being able to compute similar attractors starting from noise or training points, the trajectories in latent vector to attractors are very different, according to the source distribution considered: we show this by reporting FPR95 scores for separating trajectories from noise distribution to train distribution, based on the following measure  $score(\mathbf{z}) = \frac{1}{N} \sum_{\mathbf{z}_i \in \pi(\mathbf{z})} d(\mathbf{z}_i, \mathbf{Z}_{train}^*)$  where  $\pi(\mathbf{z}) = [\mathbf{z}_0, \dots, \mathbf{z}_N]$  is the trajectory. FPR drastically decreases with training, demonstrating that the networks achieves separability of the two distributions of trajectories.

**Takeaway:** As the latent vector field evolves during training, the model transitions from memorization to generalization, forming similar attractors from different input distributions, while retaining information of the source distribution in the latent trajectories.

## 4 Experiments on vision foundation models

In this section we demonstrate the existence and applicability of the latent dynamics on vision foundation models, including AE backbone of the Stable Diffusion model[46] variants and vision transformer masked AEs [15], showing; (i) how information stored in the weights of a pretrained model can be recovered by computing the attractors from noise (ii) how trajectories in the latent dynamics are informative to characterize the learned distribution and detect distribution shifts.

### 4.1 Data free weight probing

**Setting.** In the following experiment, our goal is to analyze to what degree we can recover information stored in the weights of a neural model from attractors computed from Gaussian noise, without relying on any input data. We focus on the analysis of the AE of stable diffusion [46] pretrained on the large scale Laion2B dataset [47]. We sample input  $\mathbf{Z}_n \sim \mathcal{N}(0, I)$  and compute the attractors corresponding to the solution of the equation  $f(\mathbf{Z}_n^*) = \mathbf{Z}_n^*$ . Specifically, we sample  $N = 4096$  points which correspond to the latent dimensionality of the model  $k$ . We evaluate the reconstruction performance on 6 different and diverse datasets Laion2B [47], Imagenet [9], EuroSAT [18], CIFAR100 [27], PatchCamelyon [30], Places365 [31], showcasing highly different distributions of images from general domains, to medical and satellite data. We evaluate on 500 test samples from each

dataset, sampled randomly, using Orthogonal Matching Pursuit (OMP) [33] to reconstruct the sample from the attractors in the latent space, as a function of the sparsity imposed by the number of atoms selected. We compare with the reconstructions from the initial orthogonal basis  $Z_0^*$ , which, when using all samples, span completely  $\mathcal{Z}$ . The reconstruction performance is measured in the output space, decoding the reconstructed latents via  $D$ .

**Analysis of results.** In Figure 4, we plot the error as a function of the number of elements (atoms) chosen to reconstruct the test samples using OMP. We compare by building a random orthogonal basis sampled in the latent space. For the latter, applying OMP corresponds to performing Principal Component Analysis (PCA) on the chosen basis. On all considered datasets, the reconstructions from noise attractors the testing points with lower reconstruction error, representing a better dictionary of signals. In Figure 4a we show qualitative reconstruction using only 5 % of the atoms. In 7, 8, 9 we include additional qualitative evidence of this phenomenon, visualizing reconstructions of random samples of the datasets as a function of the number of atoms used. In Section B, we report additional results on variants of the AE of different sizes.

**Takeaway.** Attractors of foundation models computed from noise can serve as a dictionary of signals to represent diverse datasets, demonstrating that it is possible to probe the information stored in the weights of foundation models in a black box way, without requiring any input data.

## 4.2 Latent trajectories characterize the learned distribution

In the following experiment, we test the hypothesis that trajectories are informative on the distribution learned by the model, testing how much Theorem 3.1 holds in real cases. In particular, we want to assess how much the paths in the vector field can detect distribution shifts in the data. For a sample to be classified as out-of-distribution (OOD) we identify two relevant questions to investigate: (i) does the sample iteration converge to one of the attractors of the training data, i.e., does it *share the same basin* of attraction? (ii) If so, *how fast* does it converge to the attractor? An OOD sample can, in fact, lie inside one of the attractor basins shared with training data. In order to assess this, we propose to track the distribution of distances to attractors point along the encoding-decoding iteration of a test sample. In the former case, we expect that an OOD sample converges faster, while in the latter case, the distance term to the attractors will dominate the score.

**Setting.** We test this hypothesis on the masked AE architecture ViT-MAE [15], pretrained on the Imagenet dataset. As test samples, we take  $N = 2000$  samples from the training distribution of Imagenet and compute the attractors from them, stopping the iteration with a tolerance  $1e - 5$  or a maximum number of iterations. We test on samples from the following datasets SUN397 [53], Places365, Texture[6], iNaturalist [50], benchmarks commonly employed in out-of-distribution detection benchmarks [54], and we report two metrics in our experiments: False-positive rate at %95 true positive rate (FPR95), and Area Under the Receiver Operating Characteristic Curve (AUROC). FPR95 measures what percentage of OOD data we falsely classify as ID where our threshold includes 95% of ID data.

**Analysis of results.** In Table we report OOD detection performance by using the following score function: for a test sample  $\mathbf{z}_{test}$  we compute its trajectory  $\pi_{\mathbf{z}_{test}} = [\mathbf{z}_0, \dots, \mathbf{z}_N^*]$  towards attractors and compute the distance of  $\pi_{\mathbf{z}_{test}}$  w.r.t. to the set of training attractors  $\mathbf{Z}_{train}^*$ , i.e.  $score(\mathbf{z}) = d(\pi_{\mathbf{z}_{test}}, \mathbf{Z}_{train}^*)$ . As a distance function, we employ Euclidean distance, and we aggregate the score computing the mean distance over the trajectory  $score(\mathbf{z}) = \frac{1}{N} \sum_i d(\mathbf{z}_i, \mathbf{Z}_{train}^*)$ . We compare with a  $K$ -Nearest neighbor baseline, where the score for a test sample is obtained by taking the mean distance over the  $K$ -NN on the training dataset, where  $K = 2000$  in the experiments. The score proposed demonstrates how informative the latent vector field is on the training distribution. In Figure 5 on the right, we show histograms of scores for the distance to attractors and the KNN, showing again that the former method is able to tell apart in-distribution and out-of-distribution data correctly.

**Takeaway.** Trajectories in the latent vector field characterize the source distribution and are informative to detect distribution shifts.

## 5 Related Work

**Memorization and generalization in NNs** NNs exhibit a rich spectrum of behaviors between memorization and generalization, depending on model capacity, regularization, and data availability

Method	SUN397		Places365		Texture		iNaturalist	
	FPR ↓	AUROC ↑	FPR ↓	AUROC ↑	FPR ↓	AUROC ↑	FPR ↓	AUROC ↑
<i>d(Attractors)</i>	29.60	91.20	29.95	90.99	25.85	92.63	29.85	91.29
KNN	100.00	42.59	100.00	32.36	34.50	89.41	86.35	68.60

(a) FPR and AUROC scores

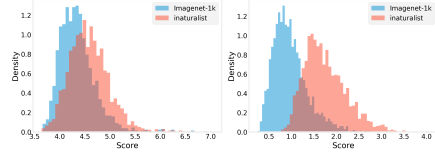


Figure 5: *Trajectories in the latent vector field characterize distribution shifts* We measure out-of-distribution detection performance on ViTMAE: On the *left* we report scores for 4 different datasets, highly outperforming the KNN baseline. On the *right* histograms of scores the INaturalist dataset demonstrating much better separability between in-distribution and out-of-distribution.

[3, 57, 40]. In the case of extreme overparametrization, namely networks trained on few data points, it has been showed experimentally in [42, 56] and theoretically for sigmoid shallow AEs in [22] that AEs can memorize examples and implement associative memory mechanisms. [2, 51]. A similar phenomenon has been observed in diffusion models in [48, 8] and analyzed in [24]. Similarly, non gradient-based approaches such as Hopfield networks and their modern variants [19, 43] extend classical attractor dynamics to neural system that interpolate between memory-based and generalizing regimes. In our work, we show that AEs fall in general in the spectrum between memorization and generalization, depending on inductive biases that enforce contraction.

**Contractive neural models:** Different approaches have been proposed to regularize NNs in order to make them smoother and more robust to input perturbations and less prone to overfitting. Many of these regularization techniques either implicitly or explicitly promote contractive mappings in AEs: for example sparse AEs [37, 12], their denoising variant [52], and contractive AEs [44, 2] losses enforce learned maps to be contractive through the loss. Regularization strategies such as weight decay [28] favor as well contractive solutions for neural models, and they are incorporated in standardized optimizers such as AdamW [32]. All these approaches enforce either directly or indirectly the existence of fixed points and attractors in the proposed latent vector field representation.

**Nonlinear operators spectral analysis** In the context of image processing and 3D graphics, previous work has inspected generalization of spectral decompositions to nonlinear operators [5, 13, 10], focusing on one homogeneous operator (e.g., p-Laplacians). In our method, the fixed points computation of the vector field can be interpreted as the decomposition of the NN into a dictionary of signals

## 6 Conclusions and Discussion

In this manuscript we proposed to represent neural AEs as vectors fields, implicitly defined by iterating the decoding encoding map in the latent space. We showed that attractors in the latent vectors fields exists in practice due to inductive biases in the training regime which enforce local contractive solutions and they retain important properties of the model and the data, linking to memorization and generalization properties of the model. We show that the information stored in the weights can be retrieved without using any input data in vision foundation models and paths in the vector field are informative to characterize the learn distribution and detect distribution shifts.

### Limitations and future works

*Generalizing to arbitrary models* Eq. 3 cannot be directly generalized to model trained with discriminative objectives such as a deep classifiers, or self supervised models, as the network is not invertible. However we note that point space the vector field is still defined in the output space, and can be simply by computing the residual  $F(\mathbf{x}) - y$ . and in the neighborhood of an attractor, the relation in proposition 1 can still hold for different objectives. An alternative intriguing idea is the one to train a *surrogate AE* model in the latent space of the model of interest, which would be agnostic from the pretraining objective. Sparse AEs for mechanistic interpretability of large language models (LLMs) [12] fit in this category. Analyzing the associated latent vector field can shed light on features learned by SAEs and biases stored in their weights.

*Learning dynamics:* characterizing how attractors forms during training, under which conditions noise attractors converge to the training attractors, holds promise to use the proposed representation to study the learning dynamics of neural models to inspect finetuning of AE modules, such as low-rank adapters [20] and double descent [36].

*Alignment of latent vector field:* Finally, following recent findings in representation alignment [35, 11, 21] inspecting how latent vector fields of networks trained are related is an open question for future works, to possibly use this representations to compare different neural models.

## Acknowledgments and Disclosure of Funding

This research was funded in whole or in part by the Austrian Science Fund (FWF) 10.55776/COE12. For open access purposes, the author has applied a CC BY public copyright license to any author accepted manuscript version arising from this submission. MF is supported as well by the MSCA IST-Bridge fellowship which has received funding from the European Union’s Horizon 2020 research and innovation program under the Marie Skłodowska-Curie grant agreement No 101034413. M.F. thanks C.Domine, V.Maiorca, I.Cannistraci, R.Cadei, B.Demirel, S.Vedula for insightful discussions.

## References

- [1] Droniou Alain and Sigaud Olivier. Gated autoencoders with tied input weights. In *International Conference on Machine Learning*, pages 154–162. PMLR, 2013.
- [2] Guillaume Alain and Yoshua Bengio. What regularized auto-encoders learn from the data-generating distribution. *The Journal of Machine Learning Research*, 15(1):3563–3593, 2014.
- [3] Devansh Arpit, Stanisław Jastrzębski, Nicolas Ballas, David Krueger, Emmanuel Bengio, Maxinder S Kanwal, Tegan Maharaj, Asja Fischer, Aaron Courville, Yoshua Bengio, et al. A closer look at memorization in deep networks. In *International conference on machine learning*, pages 233–242. PMLR, 2017.
- [4] Yoshua Bengio, Aaron Courville, and Pascal Vincent. Representation learning: A review and new perspectives. *IEEE transactions on pattern analysis and machine intelligence*, 35(8):1798–1828, 2013.
- [5] Leon Bungert, Ester Hait-Fraenkel, Nicolas Papadakis, and Guy Gilboa. Nonlinear power method for computing eigenvectors of proximal operators and neural networks. *SIAM Journal on Imaging Sciences*, 14(3):1114–1148, 2021.
- [6] Mircea Cimpoi, Subhransu Maji, Iasonas Kokkinos, Sammy Mohamed, and Andrea Vedaldi. Describing textures in the wild. In *Proceedings of the IEEE conference on computer vision and pattern recognition*, pages 3606–3613, 2014.
- [7] Francesco D’Angelo, Maksym Andriushchenko, Aditya Vardhan Varre, and Nicolas Flammarion. Why do we need weight decay in modern deep learning? *Advances in Neural Information Processing Systems*, 37:23191–23223, 2024.
- [8] Salman Ul Hassan Dar, Arman Ghanaat, Jannik Kahmann, Isabelle Ayx, Theano Papavassiliu, Stefan O Schoenberg, and Sandy Engelhardt. Investigating data memorization in 3d latent diffusion models for medical image synthesis. In *International Conference on Medical Image Computing and Computer-Assisted Intervention*, pages 56–65. Springer, 2023.
- [9] Jia Deng, Wei Dong, Richard Socher, Li-Jia Li, Kai Li, and Li Fei-Fei. Imagenet: A large-scale hierarchical image database. In *2009 IEEE conference on computer vision and pattern recognition*, pages 248–255. Ieee, 2009.
- [10] Marco Fumero, Michael Möller, and Emanuele Rodolà. Nonlinear spectral geometry processing via the tv transform. *ACM Transactions on Graphics (TOG)*, 39(6):1–16, 2020.
- [11] Marco Fumero, Marco Pegoraro, Valentino Maiorca, Francesco Locatello, and Emanuele Rodolà. Latent functional maps: a spectral framework for representation alignment. In A. Globerson, L. Mackey, D. Belgrave, A. Fan, U. Paquet, J. Tomczak, and C. Zhang, editors, *Advances in Neural Information Processing Systems*, volume 37, pages 66178–66203. Curran Associates, Inc., 2024.

- [12] Leo Gao, Tom Dupré la Tour, Henk Tillman, Gabriel Goh, Rajan Troll, Alec Radford, Ilya Sutskever, Jan Leike, and Jeffrey Wu. Scaling and evaluating sparse autoencoders. *arXiv preprint arXiv:2406.04093*, 2024.
- [13] Guy Gilboa, Michael Moeller, and Martin Burger. Nonlinear spectral analysis via one-homogeneous functionals: overview and future prospects. *Journal of Mathematical Imaging and Vision*, 56:300–319, 2016.
- [14] Xavier Glorot and Yoshua Bengio. Understanding the difficulty of training deep feedforward neural networks. In *Proceedings of the thirteenth international conference on artificial intelligence and statistics*, pages 249–256. JMLR Workshop and Conference Proceedings, 2010.
- [15] Kaiming He, Xinlei Chen, Saining Xie, Yanghao Li, Piotr Dollár, and Ross Girshick. Masked autoencoders are scalable vision learners. In *Proceedings of the IEEE/CVF conference on computer vision and pattern recognition*, pages 16000–16009, 2022.
- [16] Kaiming He, Xiangyu Zhang, Shaoqing Ren, and Jian Sun. Delving deep into rectifiers: Surpassing human-level performance on imagenet classification. In *Proceedings of the IEEE international conference on computer vision*, pages 1026–1034, 2015.
- [17] Kaiming He, Xiangyu Zhang, Shaoqing Ren, and Jian Sun. Deep residual learning for image recognition. In *Proceedings of the IEEE Conference on Computer Vision and Pattern Recognition (CVPR)*, June 2016.
- [18] Patrick Helber, Benjamin Bischke, Andreas Dengel, and Damian Borth. Eurosat: A novel dataset and deep learning benchmark for land use and land cover classification. *IEEE Journal of Selected Topics in Applied Earth Observations and Remote Sensing*, 12(7):2217–2226, 2019.
- [19] John J Hopfield. Neural networks and physical systems with emergent collective computational abilities. *Proceedings of the national academy of sciences*, 79(8):2554–2558, 1982.
- [20] Edward J Hu, Yelong Shen, Phillip Wallis, Zeyuan Allen-Zhu, Yuanzhi Li, Shean Wang, Lu Wang, Weizhu Chen, et al. Lora: Low-rank adaptation of large language models. *ICLR*, 1(2):3, 2022.
- [21] Minyoung Huh, Brian Cheung, Tongzhou Wang, and Phillip Isola. The platonic representation hypothesis. *arXiv preprint arXiv:2405.07987*, 2024.
- [22] Yibo Jiang and Cengiz Pehlevan. Associative memory in iterated overparameterized sigmoid autoencoders. In *International conference on machine learning*, pages 4828–4838. PMLR, 2020.
- [23] John Jumper, Richard Evans, Alexander Pritzel, Tim Green, Michael Figurnov, Olaf Ronneberger, Kathryn Tunyasuvunakool, Russ Bates, Augustin Žídek, Anna Potapenko, et al. Highly accurate protein structure prediction with alphafold. *nature*, 596(7873):583–589, 2021.
- [24] Zahra Kadkhodaie, Florentin Guth, Eero P Simoncelli, and Stéphane Mallat. Generalization in diffusion models arises from geometry-adaptive harmonic representations. *arXiv preprint arXiv:2310.02557*, 2023.
- [25] Diederik P Kingma. Adam: A method for stochastic optimization. *arXiv preprint arXiv:1412.6980*, 2014.
- [26] Diederik P Kingma, Max Welling, et al. Auto-encoding variational bayes, 2013.
- [27] Alex Krizhevsky, Geoffrey Hinton, et al. Learning multiple layers of features from tiny images. *University of Toronto*, 2009.
- [28] Anders Krogh and John Hertz. A simple weight decay can improve generalization. *Advances in neural information processing systems*, 4, 1991.
- [29] Yann LeCun, Léon Bottou, Genevieve B Orr, and Klaus-Robert Müller. Efficient backprop. In *Neural networks: Tricks of the trade*, pages 9–50. Springer, 2002.

- [30] Geert Litjens, Peter Bandi, Babak Ehteshami Bejnordi, Oscar Geessink, Maschenka Balkenhol, Peter Bult, Altuna Halilovic, Meyke Hermesen, Rob Van de Loo, Rob Vogels, et al. 1399 h&e-stained sentinel lymph node sections of breast cancer patients: the camelyon dataset. *GigaScience*, 7(6):giy065, 2018.
- [31] Alejandro López-Cifuentes, Marcos Escudero-Vinolo, Jesús Bescós, and Álvaro García-Martín. Semantic-aware scene recognition. *Pattern Recognition*, 102:107256, 2020.
- [32] I Loshchilov. Decoupled weight decay regularization. *arXiv preprint arXiv:1711.05101*, 2017.
- [33] S.G. Mallat and Zhifeng Zhang. Matching pursuits with time-frequency dictionaries. *IEEE Transactions on Signal Processing*, 41(12):3397–3415, 1993.
- [34] Koichi Miyasawa et al. An empirical bayes estimator of the mean of a normal population. *Bull. Inst. Internat. Statist*, 38(181-188):1–2, 1961.
- [35] Luca Moschella, Valentino Maiorca, Marco Fumero, Antonio Norelli, Francesco Locatello, and Emanuele Rodolà. Relative representations enable zero-shot latent space communication. *arXiv preprint arXiv:2209.15430*, 2022.
- [36] Preetum Nakkiran, Gal Kaplun, Yamini Bansal, Tristan Yang, Boaz Barak, and Ilya Sutskever. Deep double descent: Where bigger models and more data hurt. *Journal of Statistical Mechanics: Theory and Experiment*, 2021(12):124003, 2021.
- [37] Andrew Ng et al. Sparse autoencoder. *CS294A Lecture notes*, 72(2011):1–19, 2011.
- [38] Adam Paszke, Sam Gross, Francisco Massa, Adam Lerer, James Bradbury, Gregory Chanan, Trevor Killeen, Zeming Lin, Natalia Gimelshein, Luca Antiga, Alban Desmaison, Andreas Köpf, Edward Yang, Zach DeVito, Martin Raison, Alykhan Tejani, Sasank Chilamkurthy, Benoit Steiner, Lu Fang, Junjie Bai, and Soumith Chintala. Pytorch: An imperative style, high-performance deep learning library, 2019.
- [39] Ben Poole, Subhaneil Lahiri, Maithra Raghu, Jascha Sohl-Dickstein, and Surya Ganguli. Exponential expressivity in deep neural networks through transient chaos. *Advances in neural information processing systems*, 29, 2016.
- [40] Alethea Power, Yuri Burda, Harri Edwards, Igor Babuschkin, and Vedant Misra. Grokking: Generalization beyond overfitting on small algorithmic datasets. *arXiv preprint arXiv:2201.02177*, 2022.
- [41] Alec Radford, Jong Wook Kim, Chris Hallacy, Aditya Ramesh, Gabriel Goh, Sandhini Agarwal, Girish Sastry, Amanda Askell, Pamela Mishkin, Jack Clark, et al. Learning transferable visual models from natural language supervision. In *International conference on machine learning*, pages 8748–8763. PMLR, 2021.
- [42] Adityanarayanan Radhakrishnan, Mikhail Belkin, and Caroline Uhler. Overparameterized neural networks implement associative memory. *Proceedings of the National Academy of Sciences*, 117(44):27162–27170, 2020.
- [43] Hubert Ramsauer, Bernhard Schäfl, Johannes Lehner, Philipp Seidl, Michael Widrich, Thomas Adler, Lukas Gruber, Markus Holzleitner, Milena Pavlović, Geir Kjetil Sandve, et al. Hopfield networks is all you need. *arXiv preprint arXiv:2008.02217*, 2020.
- [44] Salah Rifai, Pascal Vincent, Xavier Muller, Xavier Glorot, and Yoshua Bengio. Contractive auto-encoders: Explicit invariance during feature extraction. In *Proceedings of the 28th international conference on international conference on machine learning*, pages 833–840, 2011.
- [45] Herbert E Robbins. An empirical bayes approach to statistics. In *Breakthroughs in Statistics: Foundations and basic theory*, pages 388–394. Springer, 1992.
- [46] Robin Rombach, Andreas Blattmann, Dominik Lorenz, Patrick Esser, and Björn Ommer. High-resolution image synthesis with latent diffusion models. In *Proceedings of the IEEE/CVF conference on computer vision and pattern recognition*, pages 10684–10695, 2022.

- [47] Christoph Schuhmann, Romain Beaumont, Richard Vencu, Cade Gordon, Ross Wightman, Mehdi Cherti, Theo Coombes, Aarush Katta, Clayton Mullis, Mitchell Wortsman, et al. Laion-5b: An open large-scale dataset for training next generation image-text models. *Advances in Neural Information Processing Systems*, 35:25278–25294, 2022.
- [48] Gowthami Somepalli, Vasu Singla, Micah Goldblum, Jonas Geiping, and Tom Goldstein. Diffusion art or digital forgery? investigating data replication in diffusion models. In *Proceedings of the IEEE/CVF conference on computer vision and pattern recognition*, pages 6048–6058, 2023.
- [49] Yang Song and Diederik P Kingma. How to train your energy-based models. *arXiv preprint arXiv:2101.03288*, 2021.
- [50] Grant Van Horn, Oisin Mac Aodha, Yang Song, Yin Cui, Chen Sun, Alex Shepard, Hartwig Adam, Pietro Perona, and Serge Belongie. The inaturalist species classification and detection dataset. In *Proceedings of the IEEE conference on computer vision and pattern recognition*, pages 8769–8778, 2018.
- [51] Pascal Vincent. A connection between score matching and denoising autoencoders. *Neural computation*, 23(7):1661–1674, 2011.
- [52] Pascal Vincent, Hugo Larochelle, Yoshua Bengio, and Pierre-Antoine Manzagol. Extracting and composing robust features with denoising autoencoders. In *Proceedings of the 25th international conference on Machine learning*, pages 1096–1103, 2008.
- [53] Jianxiong Xiao, Krista A Ehinger, James Hays, Antonio Torralba, and Aude Oliva. Sun database: Exploring a large collection of scene categories. *International Journal of Computer Vision*, 119:3–22, 2016.
- [54] Jingkan Yang, Kaiyang Zhou, Yixuan Li, and Ziwei Liu. Generalized out-of-distribution detection: A survey. *International Journal of Computer Vision*, 132(12):5635–5662, 2024.
- [55] Shuangfei Zhai, Yu Cheng, Weining Lu, and Zhongfei Zhang. Deep structured energy based models for anomaly detection. In *International conference on machine learning*, pages 1100–1109. PMLR, 2016.
- [56] Chiyuan Zhang, Samy Bengio, Moritz Hardt, Michael C Mozer, and Yoram Singer. Identity crisis: Memorization and generalization under extreme overparameterization. *arXiv preprint arXiv:1902.04698*, 2019.
- [57] Chiyuan Zhang, Samy Bengio, Moritz Hardt, Benjamin Recht, and Oriol Vinyals. Understanding deep learning (still) requires rethinking generalization. *Communications of the ACM*, 64(3):107–115, 2021.

## A Proofs and derivation

### A.1 Theorem 3.1

We report here a detailed formulation of Theorem 3.1 alongside its proof.

**Assumption A.1** (Latent marginal). Let  $p_{\text{data}}(\mathbf{x})$  be the data distribution and  $q_\phi(\mathbf{z} | \mathbf{x})$  an encoder mapping inputs  $\mathbf{x} \in \mathbb{R}^n$  to latent codes  $\mathbf{z} \in \mathbb{R}^d$ . The latent marginal density is defined as:

$$q(\mathbf{z}) = \int p_{\text{data}}(\mathbf{x}) q_\phi(\mathbf{z} | \mathbf{x}) d\mathbf{x}.$$

We assume that  $q(\mathbf{z})$  is continuously differentiable, and that its gradient  $\nabla \log q(\mathbf{z})$  and Hessian  $\nabla^2 \log q(\mathbf{z})$  are well-defined and continuous on an open domain containing  $\Omega \subseteq \mathbb{R}^d$ .

**Assumption A.2** (Fixed-point manifold). Let  $E : \mathbb{R}^n \rightarrow \mathbb{R}^d$  be an encoder and  $D : \mathbb{R}^d \rightarrow \mathbb{R}^n$  a decoder, both continuously differentiable. Define the composite map

$$f(\mathbf{z}) = E(D(\mathbf{z})) \in \mathbb{R}^d.$$

We define the fixed-point manifold of  $f$  as

$$\mathcal{M} = \{\mathbf{z} \in \mathbb{R}^d : f(\mathbf{z}) = \mathbf{z}\}.$$

**Assumption A.3** (Local contraction). There exists an open, convex set  $\Omega \subseteq \mathbb{R}^d$ , with  $\mathcal{M} \subseteq \Omega$ , and a constant  $0 < L < 1$ , such that:

$$\sup_{\mathbf{z} \in \Omega} \|J_f(\mathbf{z})\|_{\text{op}} \leq L,$$

where  $J_f(\mathbf{z}) \in \mathbb{R}^{d \times d}$  denotes the Jacobian of  $f$  at  $\mathbf{z}$ , and  $\|\cdot\|_{\text{op}}$  denotes the operator norm (i.e., largest singular value). Therefore,  $f$  is a contraction mapping on  $\Omega$ .

**Assumption A.4** (Training optimality with Jacobian regularization). Let  $f(\mathbf{z}) = E(D(\mathbf{z}))$  be as above, with  $E, D$  trained to minimize the objective:

$$\mathbb{E}_{\mathbf{x} \sim p_{\text{data}}} [\|D(E(\mathbf{x})) - \mathbf{x}\|^2 + \lambda \|J_f(E(\mathbf{x}))\|_F^2] \quad \text{for } \lambda > 0.$$

Assume the encoder is deterministic, i.e.,  $q_\phi(\mathbf{z} | \mathbf{x}) = \delta(\mathbf{z} - E(\mathbf{x}))$ , so the latent marginal satisfies:

$$q(\mathbf{z}) = \int p_{\text{data}}(\mathbf{x}) \delta(\mathbf{z} - E(\mathbf{x})) d\mathbf{x}.$$

Then  $q(\mathbf{z})$  is supported and concentrated on the fixed-point manifold  $\mathcal{M}$ , and  $f$  is locally contractive around  $\mathcal{M}$ .

**Lemma A.5** (Directional ascent of the residual field). *Under the above assumptions, for every  $\mathbf{z} \in \Omega \setminus \mathcal{M}$ , define the residual field:*

$$\mathbf{v}(\mathbf{z}) := f(\mathbf{z}) - \mathbf{z}.$$

*Then the directional derivative of  $\log q$  in direction  $\mathbf{v}(\mathbf{z})$  is strictly positive:*

$$\langle \nabla \log q(\mathbf{z}), \mathbf{v}(\mathbf{z}) \rangle > 0.$$

*Proof.* Let  $\mathbf{z} \in \Omega \setminus \mathcal{M}$  be arbitrary. Then  $f(\mathbf{z}) \neq \mathbf{z}$ , so  $\mathbf{v}(\mathbf{z}) = f(\mathbf{z}) - \mathbf{z} \neq \mathbf{0}$ . By contractiveness and training optimality,  $f(\mathbf{z})$  is closer to the fixed-point set  $\mathcal{M}$  than  $\mathbf{z}$  is. Since  $q(\mathbf{z})$  is concentrated on  $\mathcal{M}$ , we have:

$$q(f(\mathbf{z})) > q(\mathbf{z}) \quad \Rightarrow \quad \log q(f(\mathbf{z})) > \log q(\mathbf{z}).$$

We now Taylor-expand  $\log q$  at  $\mathbf{z}$  in direction  $\mathbf{v}(\mathbf{z})$ :

$$\log q(f(\mathbf{z})) = \log q(\mathbf{z}) + \langle \nabla \log q(\mathbf{z}), \mathbf{v}(\mathbf{z}) \rangle + R,$$

where  $R = \frac{1}{2} \mathbf{v}^\top(\mathbf{z}) \nabla^2 \log q(\xi) \mathbf{v}(\mathbf{z})$ , for some  $\xi$  between  $\mathbf{z}$  and  $f(\mathbf{z})$ . Since  $f$  is contractive,  $\|\mathbf{v}(\mathbf{z})\|$  is small and  $R = o(\|\mathbf{v}(\mathbf{z})\|)$ . Therefore:

$$\langle \nabla \log q(\mathbf{z}), \mathbf{v}(\mathbf{z}) \rangle > -R \quad \Rightarrow \quad \langle \nabla \log q(\mathbf{z}), \mathbf{v}(\mathbf{z}) \rangle > 0.$$

□

**Theorem A.6** (Convergence to latent-space modes). *Let Assumptions 1–4 hold. Let  $\mathbf{z}_0 \in \Omega$ , and define the iterative sequence:*

$$\mathbf{z}_{t+1} := f(\mathbf{z}_t) = E(D(\mathbf{z}_t)) \quad \text{for all } t \geq 0.$$

*Then:*

1. *The sequence  $\{\mathbf{z}_t\}$  converges exponentially fast to a unique fixed point  $\mathbf{z}^* \in \mathcal{M}$ , satisfying  $f(\mathbf{z}^*) = \mathbf{z}^*$ .*
2. *At the limit point  $\mathbf{z}^*$ , we have  $\nabla \log q(\mathbf{z}^*) = \mathbf{0}$ .*
3. *Moreover,  $\mathbf{z}^*$  is a local maximum of the density  $q$ : the Hessian satisfies*

$$\nabla^2 \log q(\mathbf{z}^*) \prec \mathbf{0},$$

*meaning that the Hessian is negative definite.*

**Proof. Step 1: Contraction and convergence.** By Assumption 3,  $f : \Omega \rightarrow \Omega$  is a contraction mapping with contraction constant  $L < 1$ . Since  $\Omega$  is convex and hence complete under  $\|\cdot\|$ , Banach’s fixed-point theorem applies. Therefore:

- There exists a unique fixed point  $\mathbf{z}^* \in \Omega$  such that  $f(\mathbf{z}^*) = \mathbf{z}^*$ .
- For any initial  $\mathbf{z}_0 \in \Omega$ , the iterates satisfy:

$$\|\mathbf{z}_t - \mathbf{z}^*\| \leq L^t \|\mathbf{z}_0 - \mathbf{z}^*\| \rightarrow 0 \quad \text{as } t \rightarrow \infty.$$

**Step 2: Stationarity of the limit.** At the fixed point  $\mathbf{z}^*$ , we have:

$$\mathbf{v}(\mathbf{z}^*) = f(\mathbf{z}^*) - \mathbf{z}^* = \mathbf{0}.$$

Assume for contradiction that  $\nabla \log q(\mathbf{z}^*) \neq \mathbf{0}$ . By continuity of  $\nabla \log q$ , there exists a neighborhood  $U \ni \mathbf{z}^*$  where  $\nabla \log q(\mathbf{z})$  stays close to  $\nabla \log q(\mathbf{z}^*)$ . Then for nearby  $\mathbf{z}$ , Lemma A.5 implies:

$$\langle \nabla \log q(\mathbf{z}), \mathbf{v}(\mathbf{z}) \rangle > 0.$$

But continuity of  $f$  and the residual  $\mathbf{v}(\mathbf{z}) \rightarrow \mathbf{0}$  implies the ascent direction vanishes at  $\mathbf{z}^*$ , which contradicts the assumption that  $\nabla \log q(\mathbf{z}^*) \neq \mathbf{0}$ . Hence, we conclude:

$$\nabla \log q(\mathbf{z}^*) = \mathbf{0}.$$

**Step 3: Local maximality.** By Lemma A.5 and Assumption 4, the sequence  $q(\mathbf{z}_t)$  is strictly increasing and converges to  $q(\mathbf{z}^*)$ . If  $\mathbf{z}^*$  were a saddle point or local minimum, there would exist a direction  $\mathbf{u} \in \mathbb{R}^d$  such that the second-order Taylor expansion yields:

$$\left. \frac{d^2}{dt^2} \log q(\mathbf{z}^* + t\mathbf{u}) \right|_{t=0} = \mathbf{u}^\top \nabla^2 \log q(\mathbf{z}^*) \mathbf{u} \geq 0,$$

which contradicts the fact that  $\mathbf{z}_t \rightarrow \mathbf{z}^*$  through ascent directions. Therefore, all second directional derivatives must be negative, implying:

$$\nabla^2 \log q(\mathbf{z}^*) \prec \mathbf{0}.$$

That is,  $\mathbf{z}^*$  is a strict local maximum of  $q$ . □

## A.2 Proposition 1

**Proposition A.7.** *We report here a detailed formulation of Theorem 1 alongside its proof.*

*Let  $f = E \circ D : \mathbb{R}^d \rightarrow \mathbb{R}^d$  be the composition of an autoencoder’s decoder  $D$  and encoder  $E$ , and define the residual vector field  $\mathbf{v}(\mathbf{z}) := f(\mathbf{z}) - \mathbf{z}$ . Consider the reconstruction loss*

$$L(\mathbf{z}) := \|f(\mathbf{z}) - \mathbf{z}\|^2.$$

*Then, the iteration  $\mathbf{z}_{t+1} = f(\mathbf{z}_t)$  corresponds locally to gradient descent on  $L$  (i.e.,  $\mathbf{v}(\mathbf{z}) \propto -\nabla_{\mathbf{z}} L(\mathbf{z})$ ) if either of the following conditions holds:*

1. The Jacobian  $J_f(\mathbf{z}) \approx \text{Id}$  (i.e.,  $f$  is locally an isometry).
2.  $\mathbf{z}$  is near an attractor point  $\mathbf{z}^*$  such that  $f(\mathbf{z}^*) = \mathbf{z}^*$  and  $J_f(\mathbf{z}^*) \approx 0$ .

*Proof.* We begin by expanding the loss:

$$L(\mathbf{z}) = \|f(\mathbf{z}) - \mathbf{z}\|^2 = \langle f(\mathbf{z}) - \mathbf{z}, f(\mathbf{z}) - \mathbf{z} \rangle.$$

Let  $\mathbf{v}(\mathbf{z}) := f(\mathbf{z}) - \mathbf{z}$ . Then,

$$L(\mathbf{z}) = \|\mathbf{v}(\mathbf{z})\|^2.$$

Now compute the gradient of  $L$ :

$$\begin{aligned} \nabla_{\mathbf{z}} L(\mathbf{z}) &= \nabla_{\mathbf{z}} (\mathbf{v}(\mathbf{z})^\top \mathbf{v}(\mathbf{z})) \\ &= 2J_{\mathbf{v}}(\mathbf{z})^\top \mathbf{v}(\mathbf{z}), \end{aligned}$$

where  $J_{\mathbf{v}}(\mathbf{z}) = J_f(\mathbf{z}) - \text{Id}$  is the Jacobian of the residual field.

So we obtain:

$$\nabla_{\mathbf{z}} L(\mathbf{z}) = 2(J_f(\mathbf{z}) - \text{Id})^\top \mathbf{v}(\mathbf{z}).$$

Therefore, if we ask whether  $\mathbf{v}(\mathbf{z}) \propto -\nabla_{\mathbf{z}} L(\mathbf{z})$ , we need:

$$\mathbf{v}(\mathbf{z}) \propto -(J_f(\mathbf{z}) - \text{Id})^\top \mathbf{v}(\mathbf{z}),$$

which simplifies to:

$$[(J_f(\mathbf{z}) - \text{Id})^\top + \alpha \text{Id}] \mathbf{v}(\mathbf{z}) = 0$$

for some  $\alpha > 0$ . This holds approximately in the two special cases:

- **Isometry:** If  $J_f(\mathbf{z}) \approx \text{Id}$ , then  $\nabla L(\mathbf{z}) \approx 0$ , so  $\mathbf{v}(\mathbf{z})$  is nearly stationary—i.e., we are at or near a local minimum.
- **Attractor:** If  $\mathbf{z} \approx \mathbf{z}^*$  with  $f(\mathbf{z}^*) = \mathbf{z}^*$  and  $J_f(\mathbf{z}^*) \approx 0$ , then:

$$\nabla L(\mathbf{z}^*) \approx -2\mathbf{v}(\mathbf{z}^*) = 0,$$

and thus  $\mathbf{z}^*$  is a fixed point and local minimum of the loss.

In these two cases, the dynamics of  $\mathbf{z}_{t+1} = f(\mathbf{z}_t)$  follow the direction of steepest descent of  $L$ , up to scaling. Higher order terms dominate influence the dynamics in the general case.

□

### A.3 Proposition 3.2

We report here a detailed formulation of Theorem 3.2 alongside its proof.

**Proposition A.8.** *Let  $f : \mathbb{R}^n \rightarrow \mathbb{R}^n$  be a differentiable function with a fixed point  $\mathbf{z}^* \in \mathbb{R}^n$  such that  $f(\mathbf{z}^*) = \mathbf{z}^*$ . Assume the Jacobian  $J_f(\mathbf{z}^*)$  has spectral norm  $\|J_f(\mathbf{z}^*)\|_\sigma = \rho < 1$ . Then, for initial point  $\mathbf{z}_0$  sufficiently close to  $\mathbf{z}^*$ , the sequence  $\{\mathbf{z}_t\}$  defined by the iteration  $\mathbf{z}_{t+1} = f(\mathbf{z}_t)$  satisfies:*

$$\|\mathbf{z}_t - \mathbf{z}^*\| \leq \|\mathbf{e}_0\| \cdot \rho^t,$$

and the number of iterations  $T$  needed to reach an error  $\|\mathbf{z}_T - \mathbf{z}^*\| \leq \epsilon$  is bounded by:

$$T \geq \frac{\log(\epsilon/\|\mathbf{e}_0\|)}{\log(\rho)}.$$

*Proof.* Let  $\mathbf{e}_t = \mathbf{z}_t - \mathbf{z}^*$  denote the error at iteration  $t$ . We are given that  $f$  is differentiable around  $\mathbf{z}^*$ , and that  $f(\mathbf{z}^*) = \mathbf{z}^*$ . Applying the first-order Taylor expansion of  $f$  around  $\mathbf{z}^*$ , we obtain:

$$f(\mathbf{z}_t) = f(\mathbf{z}^*) + J_f(\mathbf{z}^*)(\mathbf{z}_t - \mathbf{z}^*) + R(\mathbf{z}_t),$$

where  $R(\mathbf{z}_t)$  is the Taylor remainder satisfying  $\|R(\mathbf{z}_t)\| = o(\|\mathbf{z}_t - \mathbf{z}^*\|)$ . Since  $f(\mathbf{z}^*) = \mathbf{z}^*$ , this becomes:

$$\mathbf{z}_{t+1} = f(\mathbf{z}_t) = \mathbf{z}^* + J_f(\mathbf{z}^*)(\mathbf{z}_t - \mathbf{z}^*) + R(\mathbf{z}_t).$$

Thus, the error evolves as:

$$\mathbf{e}_{t+1} = \mathbf{z}_{t+1} - \mathbf{z}^* = J_f(\mathbf{z}^*)\mathbf{e}_t + R(\mathbf{z}_t).$$

For  $\mathbf{z}_t$  sufficiently close to  $\mathbf{z}^*$ , we can neglect the higher-order term  $R(\mathbf{z}_t)$  in comparison to the leading linear term. Hence, the error evolves approximately as:

$$\|\mathbf{e}_{t+1}\| \leq \|J_f(\mathbf{z}^*)\|_\sigma \cdot \|\mathbf{e}_t\| + o(\|\mathbf{e}_t\|).$$

By continuity of  $f$ , there exists a neighborhood  $\mathcal{U}$  of  $\mathbf{z}^*$  where  $\|J_f(\mathbf{z})\|_\sigma \leq \rho + \delta < 1$  for some  $\delta > 0$ . Choosing  $\mathbf{z}_0 \in \mathcal{U}$  and letting  $R(\mathbf{z}_t) = 0$  (first-order approximation), the error satisfies:

$$\|\mathbf{e}_t\| \leq \|\mathbf{e}_0\| \cdot \rho^t.$$

We now ask: for which  $T$  does  $\|\mathbf{e}_T\| \leq \epsilon$ ? We solve:

$$\|\mathbf{e}_0\| \cdot \rho^T \leq \epsilon.$$

Dividing both sides by  $\|\mathbf{e}_0\|$  and taking logarithms yields:

$$\rho^T \leq \frac{\epsilon}{\|\mathbf{e}_0\|} \Rightarrow T \cdot \log(\rho) \leq \log\left(\frac{\epsilon}{\|\mathbf{e}_0\|}\right).$$

Since  $\log(\rho) < 0$ , we reverse the inequality when dividing:

$$T \geq \frac{\log(\epsilon/\|\mathbf{e}_0\|)}{\log(\rho)}.$$

This proves that the error converges exponentially and that the number of iterations required to reach error  $\epsilon$  is lower bounded by the expression above.  $\square$

## B Additional experiments

### B.1 Bias at initialization

As stated in the method section of the main paper, To empirically measure to what extent model are contractive at initialization we sample  $N = 1000$  samples from  $\mathcal{N}(0, I)$ , and we map them through 12 different vision backbones, initialized randomly across 10 seeds. We measure the ratio between the input variance  $\sigma_{in} = 1$  and output variance  $\sigma_{out}$  and we report in Figure 6 .

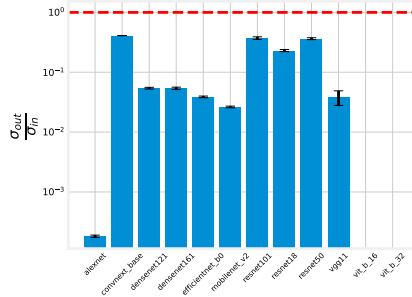


Figure 6: *Contraction at initialization* Variance preserving ratio at initialization of torchvision models: all models considered have a ratio  $< 1$ , indicating that the map at initialization is contractive.

### B.2 Qualitative results: data-free weight probing

We report additional qualitative results from the data free weight probing experiment in section 4.1, in Figures 7,8,9, observing that the reconstructions from attractors as a functions of the number of atoms used, are superior with respect to the orthogonal basis baseline.

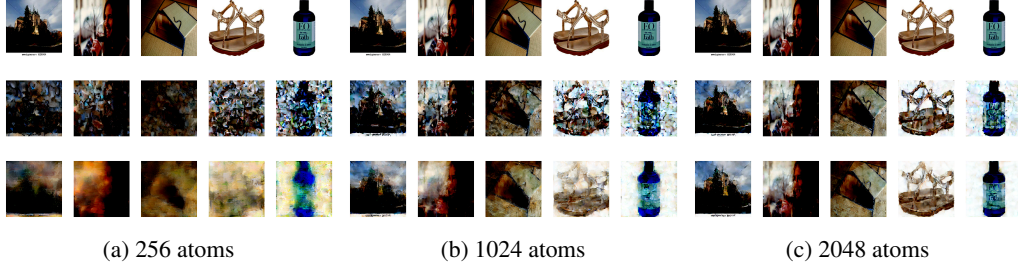


Figure 7: Visualization of reconstructions from the data-free sample recovery experiment of Figure 4: Visualizing on Laion2B reconstructions of five random samples. First row: input samples; second row: reconstructions from orthogonal basis; third row reconstructions from attractors of noise.

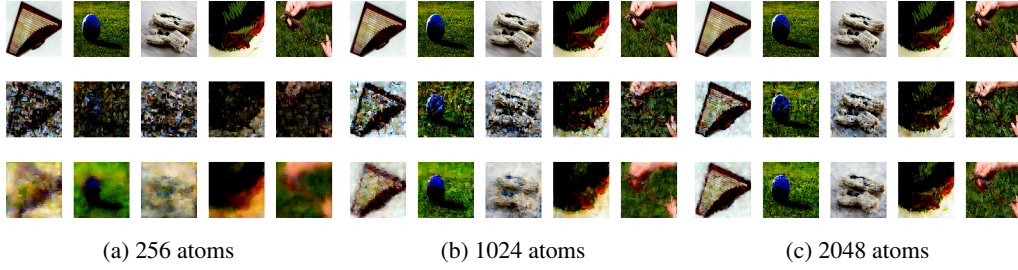


Figure 8: Visualization of reconstructions from the data-free sample recovery experiment of Figure 4: Visualizing on Imagenet1k reconstructions of five random samples. First row: input samples; second row: reconstructions from orthogonal basis; third row reconstructions from attractors of noise.

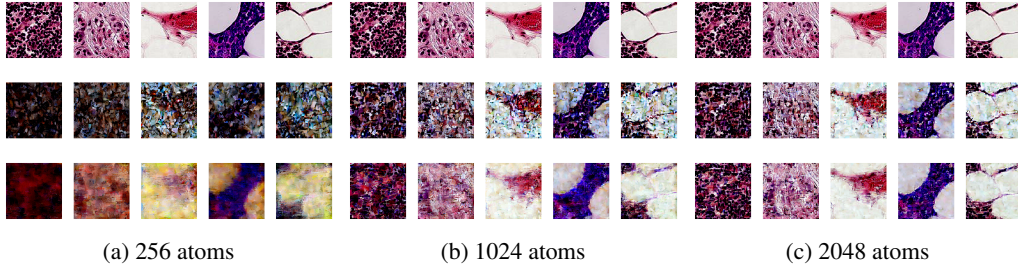


Figure 9: Visualization of reconstructions from the data-free sample recovery experiment of Figure 4: Visualizing on Camelyon17 reconstructions of five random samples. First row: input samples; second row: reconstructions from orthogonal basis; third row reconstructions from attractors of noise.

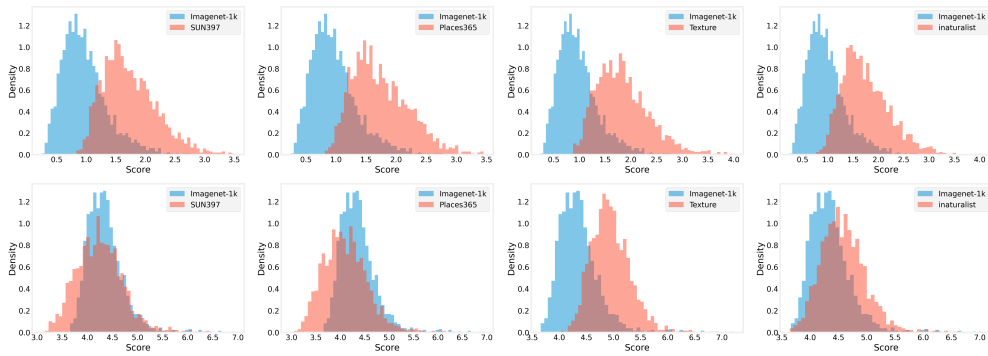


Figure 10: Histograms from OOD detections

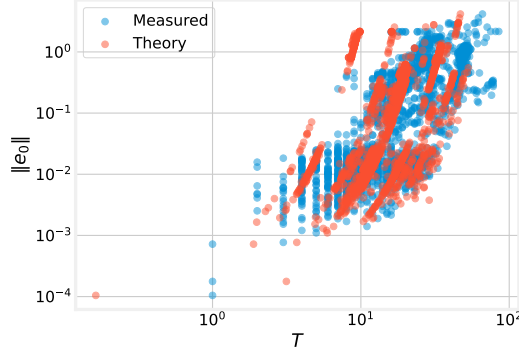


Figure 11: *Converge speed analysis* We plot the convergence speed in terms of number of iterations vs the error (distance to the attractors) of the initial condition on a convolutional autoencoders trained on MNIST. The estimated convergence has a Pearson correlation coefficient of 0.67 to the true number of iterations to converge. Higher error in the estimates occur for farer initial conditions.

### B.3 Histograms OOD detection

We report in Figure 10 additional histograms of In-Distribution vs Out-Of-Distribution scores, corresponding to the experiment in Section 4.2.

### B.4 Analysis speed of convergence

In figure 11 we report an empirical validation of proposition 3.2, for a 2 dimensional bottleneck convolution autoencoder trained on MNIST, by sampling points in the training set and measuring their convergence speed in terms of number of iteration. We remark that assumptions for the proposition don't hold for this model, as the farer an initial condition is from an attractor the more higher order terms will dominate in the dynamics, making the evaluation of the spectrum of the Jacobian at the attractor insufficient. We observe nevertheless, that the convergence speed bounds still correlates, providing a looser estimate for the number of iteration needed to converge towards an attractors with error  $\epsilon$ .

### B.5 Rank of attractor matrix

In Figure 12 we report an alternative measure of generalization of the attractors computed in the experiment in Figure 2 and in Figure 3. Specifically, we consider the matrix  $\mathbf{X}^* = D(\mathbf{Z})^*$ , and we compute its singular value decomposition  $\mathbf{U}^* \text{diag}(\mathbf{s}^*) \mathbf{V}^* = \mathbf{X}^*$ . We define the generalization entropy as the number of eigenvectors needed to explain 90% of the variance of the matrix. We report this measure for both the models employed in the experiment in Figure 2 and in Figure 3, showing that attractors are more expressive as the model generalized better, as well during training.

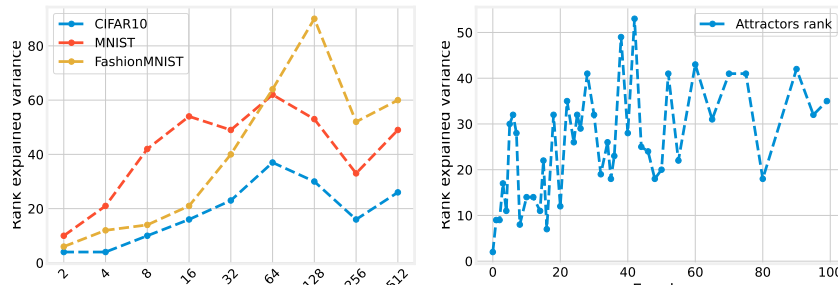


Figure 12: *Generalization increase ranks of attractors matrix*: entropy rank as a function of the bottleneck dimension (*left*) and during training, as a function of the number of epochs (*right*). Transitioning from memorization to generalization

## B.6 Memorization overfitting regime

In this section, we test the memorization capabilities of models in different (strong) overparametrization regimes, similarly as tested in [24] for diffusion models and in [42, 56] for the extremely overparametrized case (network trained on few samples). We remark that this case corresponds to an overfitting regime of the network, as opposed as underfitting (over-regularized) regime showed in the main paper. We train a convolutional autoencoder on subsamples of the CIFAR, MNIST, FashionMNIST datasets, with bottleneck dimension  $k = 128$  and weight decay  $1e - 4$ . In Figure 13 we plot the memorization coefficient as a function of the dataset size, showing that networks trained on less data (strong overparametrization) tend to memorize more the training data.

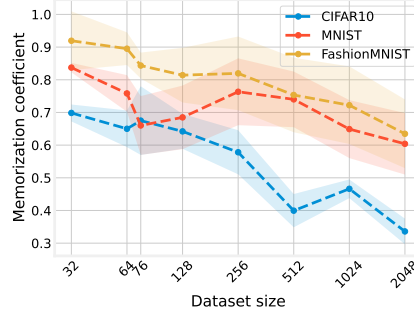


Figure 13: *Strong overparametrization favors memorization*: Memorization coefficient as a function of the dataset size on CIFAR, MNIST, FashionMNIST, showing that networks trained on less data (*strongly overparametrized*) tend to memorize more the training data.

## B.7 Data-free weight probing: additional results

We replicate the experiment in 4.1, on the larger XL version of the Stable diffusion architecture [46], observing that attractors from noise still form an informative dictionary of signals which scales better w.r.t, to a random orthogonal basis.

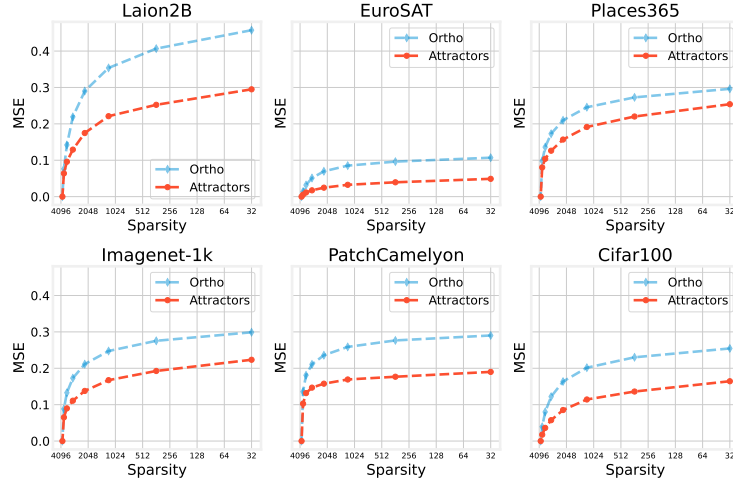


Figure 14: *Data-free weight probing Stable diffusion XL AE* : the results on the larger version of the table diffusion autoencoder confirm that attractors from noise form an informative dictionary of signals to reconstruct different datasets.

Table 1: Architecture of the AutoencoderKL in Stable Diffusion

Layer	Details	Output Shape
<b>Encoder</b>		
Input	$3 \times 256 \times 256$ image	$3 \times 256 \times 256$
Conv2D	$3 \rightarrow 128, 3 \times 3, \text{stride } 1$	$128 \times 256 \times 256$
ResNet Block	128 channels	$128 \times 256 \times 256$
Conv2D	$128 \rightarrow 256, 3 \times 3, \text{stride } 2$	$256 \times 128 \times 128$
ResNet Block	256 channels	$256 \times 128 \times 128$
Conv2D	$256 \rightarrow 512, 3 \times 3, \text{stride } 2$	$512 \times 64 \times 64$
ResNet Block	512 channels	$512 \times 64 \times 64$
Conv2D	$512 \rightarrow 512, 3 \times 3, \text{stride } 2$	$512 \times 32 \times 32$
ResNet Block	512 channels	$512 \times 32 \times 32$
Conv2D	$512 \rightarrow 512, 3 \times 3, \text{stride } 2$	$512 \times 16 \times 16$
ResNet Block	512 channels	$512 \times 16 \times 16$
Conv2D	$512 \rightarrow 512, 3 \times 3, \text{stride } 2$	$512 \times 8 \times 8$
ResNet Block	512 channels	$512 \times 8 \times 8$
Mean and Log Variance Sampling	$512 \rightarrow 4, 1 \times 1$ Reparameterization trick	$4 \times 8 \times 8$ $4 \times 8 \times 8$
<b>Decoder</b>		
Conv2D	$4 \rightarrow 512, 3 \times 3, \text{stride } 1$	$512 \times 8 \times 8$
ResNet Block	512 channels	$512 \times 8 \times 8$
Upsample	Scale factor 2	$512 \times 16 \times 16$
ResNet Block	512 channels	$512 \times 16 \times 16$
Upsample	Scale factor 2	$512 \times 32 \times 32$
ResNet Block	512 channels	$512 \times 32 \times 32$
Upsample	Scale factor 2	$512 \times 64 \times 64$
ResNet Block	512 channels	$512 \times 64 \times 64$
Upsample	Scale factor 2	$256 \times 128 \times 128$
ResNet Block	256 channels	$256 \times 128 \times 128$
Upsample	Scale factor 2	$128 \times 256 \times 256$
ResNet Block	128 channels	$128 \times 256 \times 256$
Conv2D	$128 \rightarrow 3, 3 \times 3, \text{stride } 1$	$3 \times 256 \times 256$
<b>Output: Reconstructed Image</b>		

## C Regularized autoencoder enforce contractiveness

In Table 2, we list many AE variants including denoising AEs (DAEs) [52], sparse AEs (SAEs) [37], variational AEs (VAEs) [26] and other variants [44, 2, 12] and show how their objectives enforce local contractive solutions around training points.

Autoencoder	Regularizer $\mathcal{R}_\theta(\mathbf{x})$	Description	Effect on Contractiveness
<b>Standard AE (rank <math>\leq k</math>)</b>	– (bottleneck dimension $k$ )	No explicit regularization, but dimensionality constraint induces compression	Bottleneck limits Jacobian rank: $\text{rank}(J_{f_\theta}(\mathbf{x})) \leq k$
<b>Plain AE with Weight Decay</b>	$\ \mathbf{W}_E\ _F^2 + \ \mathbf{W}_D\ _F^2$	L2 penalty on encoder and decoder weights	Reduces $\ J_{f_\theta}(\mathbf{x})\  \leq L_\sigma^2 \ \mathbf{W}_D\  \ \mathbf{W}_E\ $ by shrinking weight norms
<b>Deep AE with Weight Decay</b>	$\sum_\ell \ \mathbf{W}_E^{(\ell)}\ _F^2 + \ \mathbf{W}_D^{(\ell)}\ _F^2$	Weight decay across multiple layers of deep encoder/decoder	Layerwise shrinkage enforces smoother, more contractive composition $J_{f_\theta}(\mathbf{x})$
<b>R-Contractive AE [1]</b>	$\ J_{f_\theta}(\mathbf{x})\ _F^2$	Penalizes Jacobian of the full map $f_\theta = D_\theta \circ E_\theta$	Encourages stability of reconstructions: $f_\theta(\mathbf{x}) \approx f_\theta(\mathbf{x} + \delta)$
<b>Contractive AE [44]</b>	$\ J_{E_\theta}(\mathbf{x})\ _F^2 = \sum_{i=1}^k \ J_{E_i}(\mathbf{x})\ ^2$	Penalizes encoder Jacobian norm	Explicitly enforces local flatness of encoder
<b>Sparse AE (KL, sigmoid) [37]</b>	$\sum_{i=1}^k \text{KL}(\rho \parallel \hat{\rho}_i), \quad \hat{\rho}_i = \mathbb{E}_{\mathbf{x}}[E_i(\mathbf{x})]$	Enforces low average activation under sigmoid	Saturated units $\Rightarrow J_{E_i}(\mathbf{x}) \approx 0 \Rightarrow \ J_{E_\theta}(\mathbf{x})\ $ small
<b>Sparse AE (L1, ReLU) [37]</b>	$\ E_\theta(\mathbf{x})\ _1$	Promotes sparsity of ReLU activations	Inactive ReLU units have zero derivatives $\Rightarrow$ sparse Jacobian $J_{E_\theta}(\mathbf{x})$
<b>Denoising AE [52, 2]</b>	$\mathbb{E}_{\tilde{\mathbf{x}} \sim q(\tilde{\mathbf{x}} \mathbf{x})} \ \mathbf{x} - f_\theta(\tilde{\mathbf{x}})\ ^2$	Reconstructs from noisy input	For small noise: $f_\theta(\mathbf{x}) - \mathbf{x} \approx \sigma^2 \nabla \log p(\mathbf{x})$ , a contractive vector field $J_{f_\theta}(\mathbf{x})$
<b>Variational AE (VAE)[26]</b>	$\text{KL}(q_\theta(\mathbf{z} \mathbf{x}) \parallel p(\mathbf{z})), \quad \text{where } q(\mathbf{z} \mathbf{x}) = \mathcal{N}(\mu(\mathbf{x}), \Sigma(\mathbf{x}))$	Encourages latent distribution to match prior	Smooths $\mu(\mathbf{x}), \Sigma(\mathbf{x})$ ; penalizes sharp variations in encoder $J_\mu(\mathbf{x}), J_\Sigma(\mathbf{x})$
<b>Masked AE (MAE)[15]</b>	$\mathbb{E}_M [\ M \odot (\mathbf{x} - f_\theta(M \odot \mathbf{x}))\ ^2]$	Learns to reconstruct from partial input	Promotes invariance to missing entries $\Rightarrow \ J_{f_\theta}(\mathbf{x})\ $ low

Table 2: Unified formulation of autoencoder variants as minimizing reconstruction error plus a regularizer that encourages local contractiveness.

Table 3: Architecture of the autoencoder employed in experiments on CIFAR, MNIST, FashionMNIST datasets

Layer	Details	Output Shape
<b>Encoder</b>		
Input	$C \times H \times W$ image	$C \times H \times W$
Conv2D	$C \rightarrow d, 3 \times 3$ , stride 2, pad 1	$d \times \frac{H}{2} \times \frac{W}{2}$
Conv2D	$d \rightarrow 2d, 3 \times 3$ , stride 2, pad 1	$2d \times \frac{H}{4} \times \frac{W}{4}$
Conv2D	$2d \rightarrow 4d, 3 \times 3$ , stride 2, pad 1	$4d \times \frac{H}{8} \times \frac{W}{8}$
Conv2D	$4d \rightarrow 8d, 3 \times 3$ , stride 2, pad 1	$8d \times \frac{H}{16} \times \frac{W}{16}$
Flatten	—	$8d \cdot \frac{H}{16} \cdot \frac{W}{16}$
Bottleneck	Linear layer or projection	$z$ (latent code)
<b>Decoder</b>		
Unflatten	$z \rightarrow 8d \times \frac{H}{16} \times \frac{W}{16}$	$8d \times \frac{H}{16} \times \frac{W}{16}$
ConvTranspose2D	$8d \rightarrow 4d, 3 \times 3$ , stride 2, pad 1, output pad 1	$4d \times \frac{H}{8} \times \frac{W}{8}$
ConvTranspose2D	$4d \rightarrow 2d, 3 \times 3$ , stride 2, pad 1, output pad 1	$2d \times \frac{H}{4} \times \frac{W}{4}$
ConvTranspose2D	$2d \rightarrow d, 3 \times 3$ , stride 2, pad 1, output pad 1	$d \times \frac{H}{2} \times \frac{W}{2}$
ConvTranspose2D	$d \rightarrow C, 3 \times 3$ , stride 2, pad 1, output pad 1	$C \times H \times W$
<b>Output: Reconstructed Image</b>		

## D Additional implementation details

For the experiments in Figures 2,3, 13 we considered convolutional autoencoders with architecture specified in Table 3. We train the models with Adam [25] with learning rate  $5e - 4$ , linear step learning rate scheduler, and weight decay  $1e - 4$  for 500 epochs. For the experiments in section 4.1, we use the pretrained autoencoder of [46]. We report in Table 1 the architectural details and we refer to the paper for training details. For the experiments in section 4.2, we use the pretrained autoencoder of [15], considering the base model. We refer to the paper for training details. For computing attractors in experiments in Figures 2,3, 13, we compute the iterations  $\mathbf{z}_{t+1} = f(\mathbf{z}_t)$  until  $\|f(\mathbf{z}_{t+1}) - f(\mathbf{z}_t)\|_2^2 < 1e - 6$  or reaching  $t = 3000$ . Similarly in experiments in Sections 4.1, 4.2, we compute the iterations  $\mathbf{z}_{t+1} = f(\mathbf{z}_t)$  until  $\|f(\mathbf{z}_{t+1}) - f(\mathbf{z}_t)\|_2^2 < 1e - 5$  or reaching  $t = 500$ . All experiments are performed on a GPU NVIDIA 3080TI in Python code, using the PyTorch library [38].